Continuum Mech. Thermodyn.
https://doi.org/10.1007/s00161-024-01320-5

ORIGINAL ARTICLE

B. Cagri Sarar · M. Erden Yildizdag · B. Emek Abali

A multi-scale homogenization framework for design and strain-gradient modeling of additively manufactured parts fabricated by particulate composites

Received: 3 May 2024 / Accepted: 12 July 2024

Abstract Classical homogenization approaches applied to heterogeneous materials are suitable for the cases where a scale-separation is eminent. As the length-scale at the effective continuum reaches the length-scale of the microstructure of the material, classical homogenization approaches fail to be accurate. In such cases, higher-gradient theories may be stimulated for multi-scale material modeling of complex structures in terms of geometry and material. In this study, a multi-scale homogenization framework is presented for additively manufactured (3-D printed) composite parts with specific infill design. The overall framework consists of two major steps, namely micro-to-material and material-to-structure homogenization. In both steps, an asymptotic homogenization procedure is applied to determine constitutive parameters. In the micro-to-material homogenization, the constitutive parameters of the composite material are first determined regarding the material composition. Then, in the material-to-structure homogenization, the constitutive parameters are obtained regarding the infill design of the additively manufactured part. The developed two-step homogenization framework is applied for an off-the-shelf composite material commonly used in 3-D printers. Specifically, in this study, composite parts printed with grid infills are investigated numerically considering different infill ratios.

Keywords Additive manufacturing · Particulate media · Composites · Computational homogenization · strain-gradient elasticity

1 Introduction

Over the past decade, additive manufacturing (AM), also referred to as 3-D printing, has revolutionized the perspectives of designers and engineers, enabling fabrication of parts in terms geometric complexity, topology

B. C. Sarar
International Research Center on Mathematics and Mechanics of Complex Systems, University of L'Aquila, 67100 L'Aquila, Italy
E-mail: bekircagri.sarar@graduate.univaq.it

M. E. Yildizdag (✉)
Faculty of Naval Architecture and Ocean Engineering, Istanbul Technical University, 34469 Istanbul, Turkey
E-mail: yildizdag@itu.edu.tr

M. E. Yildizdag
Department of Architecture, Design and Urban Planning, University of Sassari, 07041 Alghero, Italy

B. E. Abali
Division of Applied Mechanics, Department of Materials Science and Engineering, Uppsala University, Box 35, 751 03 Uppsala, Sweden
E-mail: b.emek.abali@angstrom.uu.se

Published online: 29 August 2024

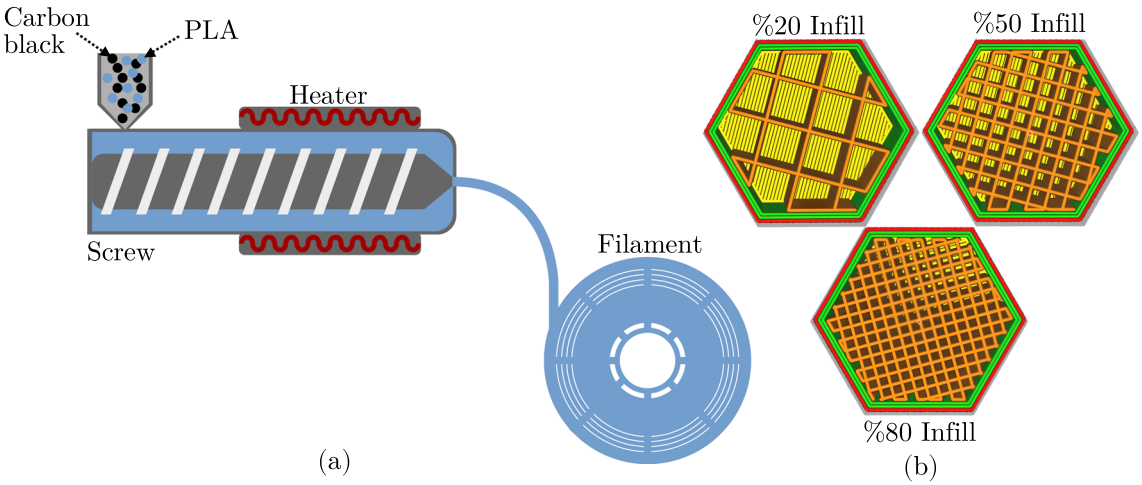

Fig. 1 **a** An illustration of composite filament extrusion by hot compression of PLA (Polylactic acid) particles and CB (carbon black) particles. **b** Infill variation for grid microstructure

optimization, multifunctionality [1], and customization. Layer-wise fabrication approaches adapted in AM considerably circumvent typical design and fabrication constraints encountered in conventional fabrication techniques, allowing for the fabrication of parts with specific internal structural patterns such as [2]. In this way, application-tailored parts can be precisely fabricated, leveraging design flexibility and material efficiency. Due to their distinctive properties, AM techniques are currently drawing great deal of interest in different fields for novel industrial applications.

One of the exceptional advantages of AM is that topologically-optimized parts can be fabricated without requiring extra complication, controlling infill pattern [3] during the tool planning process (i.e., slicing). In this way, parts can be designed along with their internal structural hierarchy in detail to attain optimal performance and properties. Here, the overall behavior is considerably affected not only due to the print material but also the infill pattern and infill ratio. In AM applications, common print materials are thermoplastics like PLA, ABS, PEEK and PETG. Besides, composite print materials like iron or carbon-filled PLA have recently become popular in AM to enhance mechanical, thermal and electromagnetic properties of 3-D printed parts, especially in material extrusion (MEX) based AM applications. To prepare such composite print materials for MEX applications, PLA or any other thermoplastic polymer is mixed as pellets with an inclusion such as iron or carbon particles and extruded as a filament described in Fig. 1, left.

The distribution of these inclusions are not controlled. Depending on their surface characteristics, some agglomeration may occur and their distribution is assumed to be random. Then, the composite filament is used in fabrication extracting the molten filament through a nozzle, which is the main mechanism in an MEX based printer. To fabricate parts by such composite print materials, overall behavior needs to be predicted accordingly. From a numerical modeling standpoint, this is a highly challenging task in terms of material properties and the geometry of the infill design (i.e., structural hierarchy) as there are different microstructures for the printed part. One microstructure is due to the composite material, randomly distributed particles embedded in a polymer. Another microstructure is because of the infill pattern and infill ratio chosen by the user during tool planning process that affects the material behavior [4]. Here, infill ratio is usually justified by weight optimization. In a general sense, an ordered porosity is introduced by a cellular design that is also found in nature to a large extent [5], inspiring researchers to develop biomimicking structures (for example, see [6,7]). Infill pattern, on the other hand, characterizes the internal structural design of 3-D printed parts to control the mechanical behavior which is one of the pattern types shown in Fig. 1, right. Also, it must be remarked that processing parameters may play a vital role for the overall print quality and must be determined accordingly depending on the print material [8].

To model and investigate overall behavior of heterogeneous media, homogenization techniques have been extensively studied in the literature. An homogenization procedure is a mathematical method for examining the behavior of materials at various length scales. The behavior of a heterogeneous material with small-scale variability in its properties is accurately captured using effective macroscopic attributes that are derived using homogenization procedures (e.g., see [9–12]). The central drawback of traditional homogenization is that it

loses accuracy for materials with scale separation between their underlying heterogeneity's size and spacing [13–15]. As the analysis in [16] shows, the microstructure introduces additional effective coefficients at the macro-scale during homogenization. Since these effective coefficients depend on the microstructure of the material, their values vary depending on the scale [17] and type of analysis performed [18]. To overcome such issues, micropolar, micromorphic [19], and strain gradient modeling approaches [20–23] may be used to accurately capture phenomena related to "size effect" as focused in [24]. Such advanced modeling techniques [25–28] are currently trending due to the recent advancements in material and manufacturing technologies to design complex structures. Specifically, strain-gradient modeling approaches have come to prominence, along with variational formulations [29–33], to model complex materials and applied into different fields. Determining effective strain-gradient constitutive parameters by using homogenization is clearly challenging [34–37]. In strain-gradient theory, hundreds of new coefficients need to be calculated. Yet for higher-order formulations, an accurate model of the macroscopic behavior is feasible not only by considering the local deformation but also the spatial variation of the deformation field namely incorporating into the homogenized model some kind of nonlocal information as presented in [38–42]. Strain gradient elasticity defines materials behavior as a continuous medium [43,44] rather than as a collection of discrete particles or pieces as studied in [45–49]. The strain gradient elasticity theory introduces additional degrees of freedom that capture the effects of microstructure on the mechanical behavior of the material over a variety of length scales, extending the classical theory of elasticity to include the effects of material microstructure [50,51] and non-local interactions [52,53]. According to the hypothesis, stress, and strain are influenced by both local deformation and the deformation gradients at nearby sites. This non-locality is constructed by simple springs connecting the next neighbors and homogenized to obtain a higher order continuum by Schödinger for the first time, we refer to [54].

In this study, we present a multi-scale homogenization framework based on strain-gradient modeling to predict the overall mechanical behavior of 3-D printed parts fabricated by composite print materials. The overall framework is divided into two parts. In micro-to-material homogenization, constitutive parameters of the composite material is determined at material scale. Then, in material-to-structure homogenization, constitutive parameters of the additively-manufactured part are determined according to its infill properties (infill pattern and infill ratio) at structure scale. As there are different length-scales in the target problem, we emphasize that the length-scales are in the same order of magnitude such that a scale separation is challenging to justify. Hence, we model from the microscale to the macroscale with the least assumptions possible and open up a discussion for a multiscale modeling by using generalized continua. In the developed framework, we take 3 different length-scales into account: micro, meso, and macro. Microscale is the composite level where the particles introduce a heterogeneous material behavior. Mesoscale represents the infill ratio related heterogeneous material. Macroscale represents the functional part printed and modeled as a homogeneous continuum. The two-step homogenization is performed based on the asymptotic homogenization procedure presented by Abali and Barchiesi [55] to determine the effective strain-gradient parameters at each step. We call the developed approach bottom-up as one begins at the composite level and use a modeling up to the part level. To show the applicability of the developed framework, we present a select numerical experiment involving parts fabricated by carbon black-filled PLA filaments with grid infill pattern.

The rest of the paper is outlined as follows. In Sect. 2, the adapted computational homogenization technique is presented, followed by the details of the overall numerical framework in Sect. 3. Then, in Sect. 4, the select numerical experiment is presented for parts printed by iron-filled PLA filaments with grid infill pattern. Finally, conclusions are drawn in Section 5.

2 Multiscale homogenization framework

The two-step multiscale homogenization approach is performed utilizing the methodology presented in [55] and verified with applications in [56–58]. The central theme of the adapted asymptotic homogenization is the equivalence of the deformation energies between the considered length-scales. Here, to summarize the formulation, the considered length-scales that the homogenization is applied between are referred to as micro and macro, respectively. Displacement, strain, stress and even energy density may differ between micro- and macro-scales on each position, but the external work remains the same for models at both scales. As the deformation is purely elastic, the applied work is used for deformation such that the following assumption is introduced

$$\int_\Omega w^{\mathrm{m}} \,\mathrm{d}V = \int_\Omega w^{\mathrm{M}} \,\mathrm{d}V \,, \tag{1}$$

for the whole body or repeating microstructure, Ω, denoting a Representative Volume Element (RVE). Here, the microstructure is denoted by a superscript "m" and its corresponding homogenized continuum is represented as superscript "M." We use the same computational domain, Ω, at both scales: at the microscale, the first-order theory models the detailed microstructure; at the macroscale, a second-order theory models a homogenized continuum. As a second-order theory, herein, we use strain-gradient elasticity.

The first-order theory is used to define a quadratic stored energy density at the microscale,

$$w^{\mathrm{m}} = \frac{1}{2}\epsilon^{\mathrm{m}}_{ij} C^{\mathrm{m}}_{ijkl} \epsilon^{\mathrm{m}}_{kl} \,, \tag{2}$$

where we use EINSTEIN's summation convention over repeated indices and C^{m}_{ijkl} is positive definite meaning the resulting scalar value for any non-zero strain value is strictly positive in each coordinate. The components are given for the microstructure with the usual symmetry conditions, $C^{\mathrm{m}}_{ijkl} = C^{\mathrm{m}}_{jikl} = C^{\mathrm{m}}_{ijlk}$. In the homogenized continuum, the simplest second-order model results from a TAYLOR expansion such that the deformation energy density reads

$$w^{\mathrm{M}} = \frac{1}{2}\varepsilon^{\mathrm{M}}_{ij} C^{\mathrm{M}}_{ijkl} \varepsilon^{\mathrm{M}}_{kl} + \varepsilon^{\mathrm{M}}_{ij} G^{\mathrm{M}}_{ijklm} \varepsilon^{\mathrm{M}}_{kl,m} + \frac{1}{2}\varepsilon^{\mathrm{M}}_{ij,k} D^{\mathrm{M}}_{ijklmn} \varepsilon^{\mathrm{M}}_{lm,n} \,, \tag{3}$$

with obvious restictions, $C^{\mathrm{M}}_{ijkl} = C^{\mathrm{M}}_{jikl} = C^{\mathrm{M}}_{ijlk}$, $D^{\mathrm{M}}_{ijklmn} = D^{\mathrm{M}}_{jiklmn} = D^{\mathrm{M}}_{ijkmln}$, $G^{\mathrm{M}}_{ijklm} = G^{\mathrm{M}}_{jiklm} = G^{\mathrm{M}}_{ijlkm}$, as well as some conditions similar to positive definiteness [59,60]. Comma notation indicates a partial derivative in space. We emphasize that $G^{\mathrm{M}} = 0$ in the case of a centro-symmetric microstructure. For the sake of simplicity in homogenization, linearized strain measure is used at both scales,

$$\varepsilon^{\mathrm{m}}_{ij} = \frac{1}{2}\left(u^{\mathrm{m}}_{i,j} + u^{\mathrm{m}}_{j,i}\right), \quad \varepsilon^{\mathrm{M}}_{ij} = \frac{1}{2}\left(u^{\mathrm{M}}_{i,j} + u^{\mathrm{M}}_{j,i}\right). \tag{4}$$

By following the asymptotic homogenization methodology as in [55], we introduce an expansion around the value at the geometric center, $\overset{c}{X} = \frac{1}{V}\int_\Omega X dV$, and involving quadratic terms as well. In conventional homogenization approaches, only linear terms are involved; however, by increasing the complexity, we may model the microstructure with the expense of higher gradients. Briefly, we solve first

$$\frac{\partial}{\partial y_j}\left(C^{\mathrm{m}}_{ijkl} L_{abkl}\right) = 0, \qquad L_{abkl} = \delta_{ak}\delta_{bl} + \frac{\partial \varphi_{abk}}{\partial y_l}.$$

where the unknown rank 3 tensor, $\boldsymbol{\varphi}$, is computed for the RVE at the microscale with given C^{m}. After the simulation, we construct

$$C^{\mathrm{M}}_{abcd} = \frac{1}{V}\int_\Omega C^{\mathrm{m}}_{ijkl} L_{abij} L_{cdkl} \, \mathrm{d}V \tag{5}$$

where C^{M} are homogenized parameters of the first-order theory. Such an approach is the outcome of a classical homogenization method used in laminate theory. We go beyond the first-order theory and compute a rank 4 tensor, $\boldsymbol{\psi}$, as a solution to the following governing equation:

$$\begin{aligned} &- C^{\mathrm{M}}_{icab} + C^{\mathrm{m}}_{ickl} L_{abkl} + \frac{\partial}{\partial y_j}\left(C^{\mathrm{m}}_{ijkl} N_{abckl}\right) = 0 \\ &N_{abckl} = \varphi_{abk}\delta_{cl} + \frac{\partial \psi_{abck}}{\partial y_l}. \end{aligned} \tag{6}$$

$\boldsymbol{\varphi}$ and $\boldsymbol{\psi}$ that are functions of y, representing spatial coordinates introduced as part of the decomposition. By using $\boldsymbol{\varphi}$ and $\boldsymbol{\psi}$, we obtain

$$M_{abcij} = y_c L_{abij} + N_{abcij} \tag{7}$$

which is used to determine all strain gradient parameters

$$
\begin{aligned}
G^{\mathrm{M}}_{abcde} &= \frac{\epsilon}{V}\int_{\Omega} C^{\mathrm{m}}_{ijkl} L_{abij} M_{cdekl}\,\mathrm{d}V \\
D^{\mathrm{M}}_{abcdef} &= \frac{\epsilon^2}{V}\left(\int_{\Omega} C^{\mathrm{m}}_{ijkl} M_{abcij} M_{defkl}\,\mathrm{d}V - C^{\mathrm{M}}_{abde}\int_{\Omega} y_c y_f\,\mathrm{d}V\right).
\end{aligned}
\tag{8}
$$

We observe that C^{M}, G^{M}, and D^{M} depend on ϵ^0, ϵ^1, and ϵ^2, respectively.

In this methodology, with the known microscale material parameters, C^{m}, for a heterogeneous continuum; we determine macroscale constitutive parameters, C^{M}, G^{M}, D^{M}, for a homogenized continuum. Notably, the numerical solution of Eqs. (5) and (6) follows the standard finite element method procedure. We use a finite-dimensional Hilbertian Sobolev space for both the trial and test functions, employing the Galerkin method. The structure is discretized using tetrahedral elements, and the discrete problem is solved by minimizing the weak form. Thus, we solve the governing equations by converting them to a weak form, obtained by multiplying by the corresponding test function and integrating by parts. For $\boldsymbol{\phi}$ from Eq. (5), we obtain 6 different weak forms and for $\boldsymbol{\psi}$ from Eq. (6) we obtain 18 different weak forms in the three-dimensional case, by separately choosing a,b,c indices as 1,2,3, concretely,

$$
\int_{\Omega} C^{\mathrm{m}}_{ijkl} L_{abkl} \frac{\partial \delta\varphi_{abi}}{\partial y_j}\,\mathrm{d}V = 0, \tag{9}
$$

$$
\int_{\Omega}\left(-C^{\mathrm{M}}_{icab}\delta\psi_{abci} + C^{\mathrm{m}}_{ickl} L_{abkl}\delta\psi_{abci} - C^{\mathrm{m}}_{ijkl} N_{abckl}\frac{\partial \delta\psi_{abci}}{\partial y_j}\right)\mathrm{d}V = 0. \tag{10}
$$

We approximate all analytical functions by a discrete representation as usual in the Finite Element Method (FEM) with form functions having a compact support [61]. Hence, monotonous convergence is guaranteed. Specifically, we span a finite dimensional HILBERTian SOBOLEV space for trial and test functions. As known as the GALERKIN approach, the same space is used for trial and test functions. Trial functions, $\boldsymbol{\varphi}$ and $\boldsymbol{\psi}$, and their corresponding test functions, $\delta\boldsymbol{\varphi}$ and $\delta\boldsymbol{\psi}$, are all approximated by linear form functions, also known as linear LAGRANGE elements. The computational domain is the RVE and periodic boundary conditions are applied on all boundaries. The domain is discretized by nodes and their connectivity by elements, this so-called triangulation [62] has been established by NetGen algorithms in Salome CAD software. We stress that Salome is allowing a Python script to build random distribution and mesh allowing an automatized preprocessing for a study. Since micro-, meso-, and macroscales are all expressed in the same coordinate system, we use the same discretized space within the domain. We use open-source packages known as FEniCS for matrix assembly and solving by using PetSc packages (with a Mumps solver). We refer to [63] for engineering applications and their implementation in FEniCS.

The developed two-step homogenization framework utilizes above-mentioned asymptotic homogenization procedure and the overall framework is illustrated in Fig. 2. The homogenization is performed from the composite level to the structure level to determine the constitutive parameters of the printed part. The first step, referred to as micro-to-material homogenization, determines the constitutive parameters (C^{M}, D^{M}) of the particulate print material according to particle volume fraction. In the subsequent analysis, which is referred to as material-to-structure homogenization, constitutive parameters at the structure level (C^{S} and D^{S}) are determined by employing constitutive materials at material level determined in the previous analysis. Here, it should be remarked that only the constitutive parameters of first-order theory (C^{M}) are considered in the micro-to-material homogenization step as the parameters of second-order theory do not play a significant role. The constitutive parameters C^{S} and D^{S} are determined according to the infill pattern and infill ratio of the printable sample.

3 Numerical experiment

To show the applicability of the developed homogenization framework, additively-manufactured parts fabricated by carbon black (CB)-filled PLA filament are considered in the numerical study. It is assumed that the filament has 20% volume fraction of carbon black, where PLA is of YOUNG's modulus $E_1 = 3.5$ GPa and POISSON's ratio $\nu_1 = 0.3$, and CB is of YOUNG's modulus $E_2 = 210$ GPa and POISSON's ratio $\nu_2 = 0.3$.

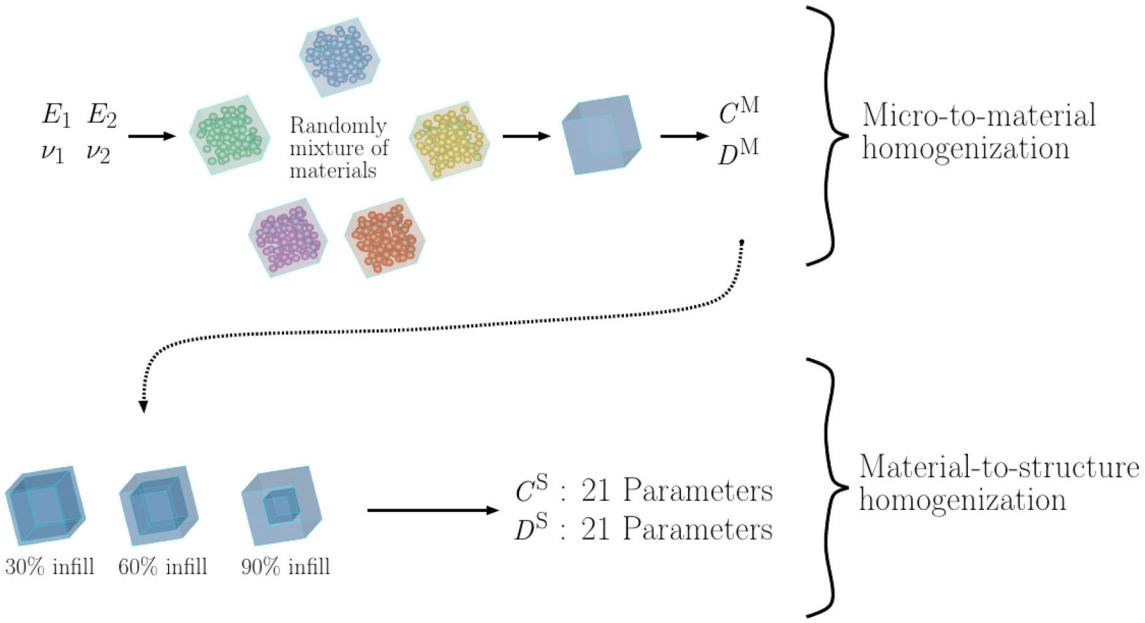

Fig. 2 Two-step asymptotic homogenization

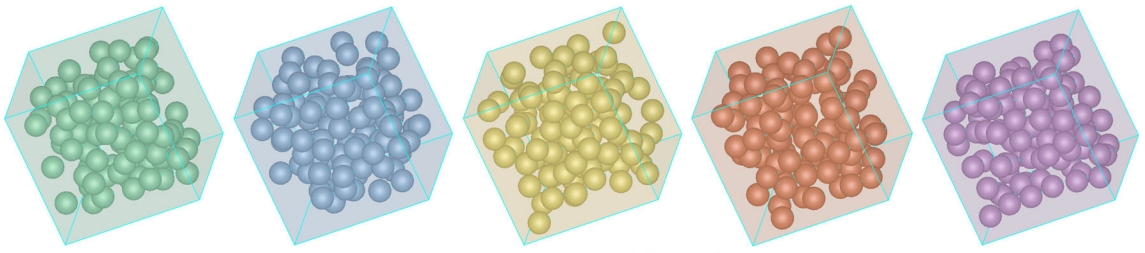

Fig. 3 Representative volume elements consisting of PLA (matrix) and 100 randomly distributed carbon blacks (inclusion) in equal radius

The micro-to-material homogenization (Fig. 2) is performed by defining a cubic RVE of PLA with 100 randomly distributed CB particles. The radius of the spherical CB particles is 0.1 mm, which is an acceptable size for commercial composite filaments. The number of particles has been determined by a pre-study to set the minimum number of particles representing the randomized distribution, adequately. To this end, we have used the same volume fraction and increased the number of particles systematically, say, 10, 20, 30... With 100 particles, 5 simulations, each with a different (random) distribution, result the "same" solution. In each simulation, a different RVE is generated in terms of particle distribution with linear tetrahedral elements, assigning a characteristic length of 0.05 mm of maximum size. Also, the number of nodes (degrees of freedom) for five different representative volume elements (RVEs) are as follows: 31957 (89169), 34154 (95760), 31671 (88311), 29032 (80394), and 33918 (95052). Importantly, as periodic boundary conditions are applied for the homogenization, the opposite faces of RVE are constrained to have the same discretization. Also, we have used less than 5% difference as a rule of thumb to accept that solutions are the same. Roughly speaking, the numerical (discretization) error has been fixed to below 1% by a standard convergence analysis. In the end, when 100 particles are randomly distributed, the solution is within the set tolerance. We construct the particles by allowing them to touch each other at a maximum of 5% volume. In reality, such a condition is generated by a surface functionalization to prevent agglomeration in manufacturing. But around 5% of allowance to touch has been found reasonable by observing microscopic images of commercially available filaments. During RVE generation, each run results in different unit cells since the distribution is random with conditions of volume fraction and contact allowance. Five generated domains, each with side lengths of 1.28 mm - resulting from the assigned particle radius of 0.1 mm and a volume fraction of 20%-are depicted in Fig. 3.

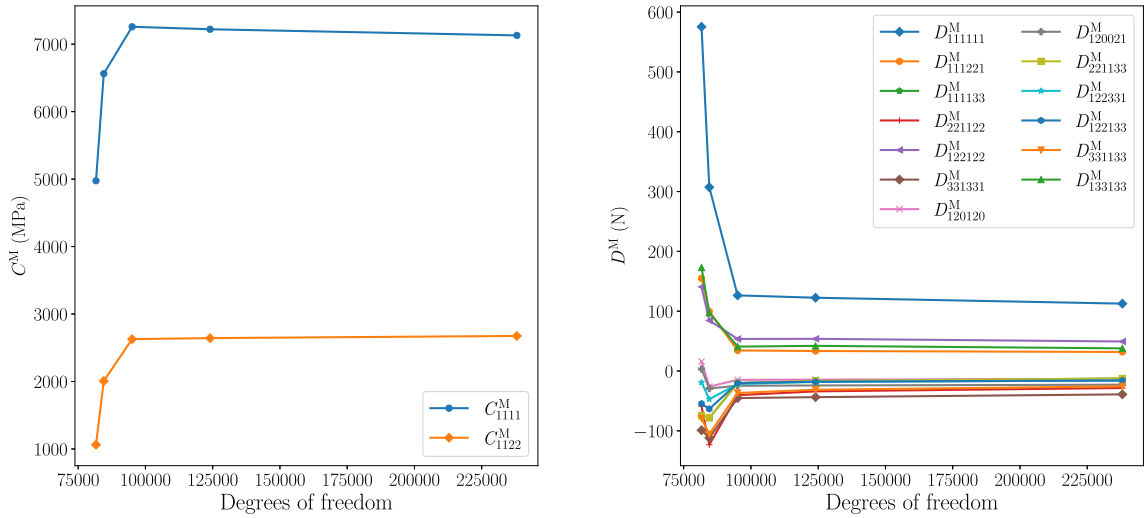

Fig. 4 Convergence analysis regarding constitutive parameters for one randomly generated RVE composed of PLA and CB on the ordinate and the total number of degrees of freedom on the abscissa

In Fig. 4, the performed convergence analysis is presented according to the number of degrees of freedom(DOFs) to determine all non-zero constitutive parameters (C^{M} and D^{M}) at the material scale. The convergence analysis was conducted using five different discretizations. As expected, we observe a monotonous convergence for parameters at the material scale. Also, all parameters in G^{M} are numerically zero. Here, we circumvent ourselves from predicting the outcome and compute all these parameters.

A further analysis reveals that D^{M} may be neglected for the micro-to-material homogenization. Regarding the components of the calculated rank 4 tensor, C^{M}, and rank 6 tensor, D^{M}, we conclude that higher-order constitutive parameters are unnecessary for the chosen RVE length. The SI unit of the parameters in the rank 6 tensor is N and the SI unit of the parameters in the rank 4 tensor is N mm^{-2}. The square root of the ratio of the units of these components is mm, which is the length-scale where the higher-order parameters start dominating the result. The square root of the ratio between the maximum value of the rank 6 tensor and the maximum value of the rank 4 tensor is approximately 0.13 mm, which is one order of magnitude smaller than the RVE size of 1.28 mm. Thus, strain-gradient parameters are not necessary, and only the constitutive parameters of C^{M} are considered effective at the material scale. The averaged and rounded effective constitutive parameters of CB-PLA composite are as follows:

$$C^{\mathrm{M}} = \begin{pmatrix} 7300 \pm 58 & 2600 \pm 33 & 2600 \pm 32 & 0 & 0 & 0 \\ 2600 \pm 33 & 7400 \pm 114 & 2600 \pm 22 & 0 & 0 & 0 \\ 2600 \pm 32 & 2600 \pm 22 & 7400 \pm 101 & 0 & 0 & 0 \\ 0 & 0 & 0 & 2300 \pm 49 & 0 & 0 \\ 0 & 0 & 0 & 0 & 2300 \pm 76 & 0 \\ 0 & 0 & 0 & 0 & 0 & 2300 \pm 58 \end{pmatrix} \text{MPa} \tag{11}$$

where we use the standard VOIGT notation. Calculated constitutive parameters in the VOIGT notation fit the isotropic symmetry class as verified in [64,65] and explained in detail in [57].

For the material-to-structure homogenization, it is assumed that the additively manufactured parts have grid-type infill pattern, and different infill ratios are considered as shown in Fig. 5.

Each RVE to perform material-to-structure homogenization consists of CB-PLA and void. For CB-PLA, we use the parameters given in Eq. (11), and we define a dummy material with a modulus of 0.001 MPa for the void part of RVE. Numerically, the void part cannot be chosen as a zero stiffness in order to obtain an FEM matrix that is solvable. Here, we repeated practically the same approach using the strain-gradient theory to determine the constitutive parameters (C^{S} and D^{S}). At least 3 RVE of 1.28 mm is necessary to achieve a homogenized continuum [66], thus, we have selected in all the simulations, cubic RVEs of side length 5 mm. In Fig. 6, the performed convergence analysis at the structure scale is presented for 70% infill ratio, considering five levels of discretization. The discretization level for a 70% infill ratio results in varying numbers of nodes (linear tetrahedral elements) across five levels: 4581 nodes (21199 elements), 10846 nodes (53427 elements),

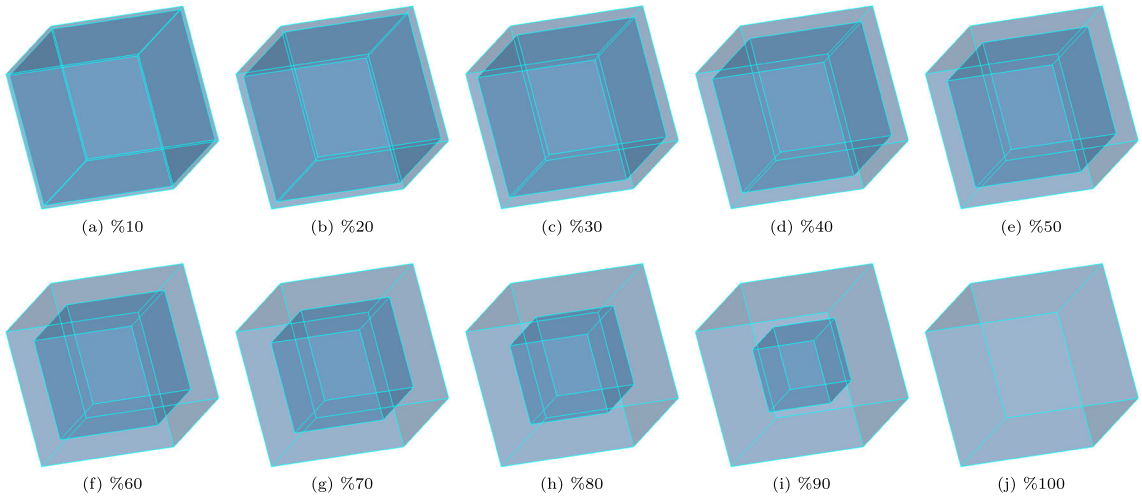

Fig. 5 Grid pattern and resulting RVE for computed infill ratios, transparency is used to show the material (light blue) and void (dark blue) parts

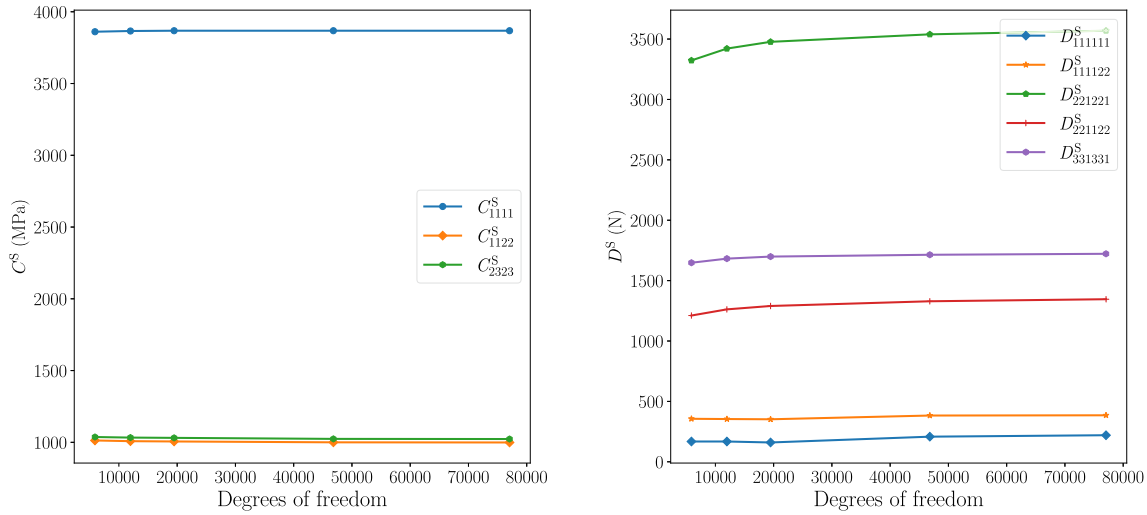

Fig. 6 Mesh convergence of an RVE with 70% infill ratio for the computed macroscale parameters, C^S, D^S

21485 nodes (105094 elements), 39195 nodes (196263 elements), and 76526 nodes (422738 elements). The corresponding degrees of freedom are 11139, 27528, 54411, 100713, and 205656, respectively. It is clear that all the non-zero constitutive parameters converge at the structure scale.

Importantly, the ratio of rank 6 tensor parameters, D^S, to rank 4 tensor parameters, C^S, are around 1 mm, therefore, the strain gradient is not negligible for an RVE of side length 5 mm. The effect of second-gradient is weaker than the first-gradient components. This result is often the case, unless a special type of microstructure with mechanisms are constructed [33,67–70].

In Fig. 7, all the predicted non-zero constitutive parameters (those of C^S ad D^S) are presented as functions of infill ratio. The chosen RVE has a cubic symmetry class, yet we compute all parameters without taking any symmetry class assumptions and obtain results matching the expected number of independent components for a cubic symmetry. In the cubic symmetry, the number of rank 6 tensor's independent constitutive parameters is 11 while there are 3 rank 4 tensor parameters. Also all rank 5 tensor parameters are computed but they are numerically zeros as expected from this cubic symmetry that is centro-symmetric.

We emphasize that limit cases of 0% or 100% infill ratio creates an already homogenized continuum such that the microstructure vanishes such as $D^S = 0$. Therefore, the values between 0-100% have an optimum (maximum or minimum) value. This feature is quite important for a tailored material design at the structure scale. In the case of a monotonous change, an optimization is more topological but not microstructural. For

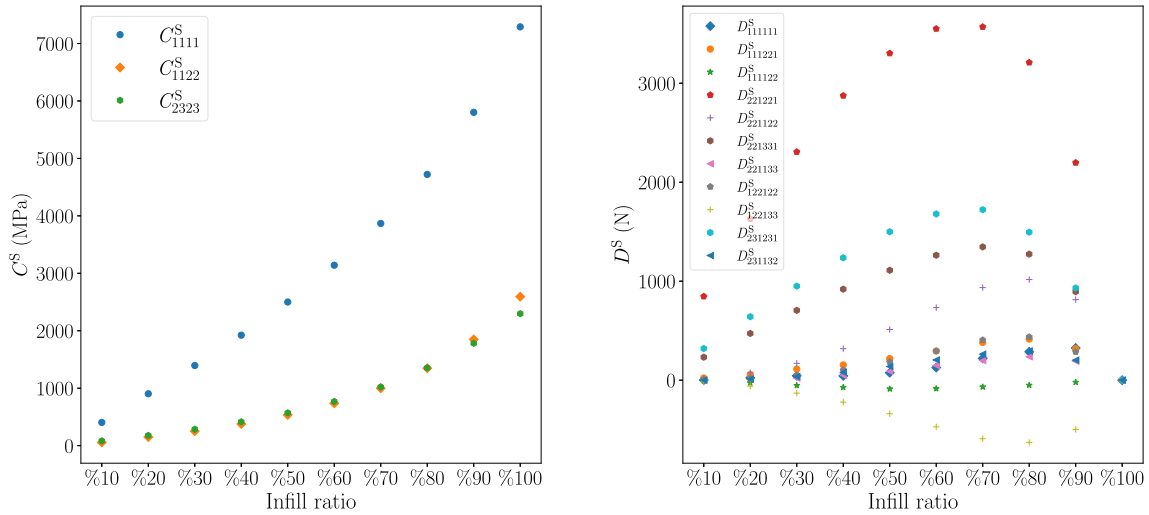

Fig. 7 Computed macroscale parameters for varying infill ratio

Table 1 Coefficients of polynomial fit functions for all parameters in the form of $P(\alpha) = A\alpha^6+B\alpha^5+C\alpha^4+D\alpha^3+E\alpha^2+F\alpha+G$ regarding the infill ratio, α

	A	B	C	D	E	F	G
C^S_{1111}	0	0	$8.00 \cdot 10^3$	$-1.05 \cdot 10^4$	$6.26 \cdot 10^3$	$3.50 \cdot 10^3$	2.86
C^S_{1122}	0	0	$4.55 \cdot 10^3$	$-5.52 \cdot 10^3$	$3.33 \cdot 10^3$	$2.13 \cdot 10^2$	2.99
C^S_{2323}	0	0	$7.69 \cdot 10^2$	$5.91 \cdot 10^2$	$8.94 \cdot 10$	$8.53 \cdot 10^2$	-1.77
D^S_{111111}	$-1.79 \cdot 10^4$	$3.51 \cdot 10^4$	$-2.23 \cdot 10^4$	$3.47 \cdot 10$	$-2.74 \cdot 10$	$5.17 \cdot 10$	-1.10
D^S_{111221}	$8.33 \cdot 10^3$	$-3.30 \cdot 10^4$	$4.15 \cdot 10^4$	$-2.22 \cdot 10^4$	$5.62 \cdot 10^3$	$-2.01 \cdot 10^2$	0.72
D^S_{111122}	0	0	$-1.21 \cdot 10^3$	$2.63 \cdot 10^3$	$-1.50 \cdot 10^3$	$6.75 \cdot 10$	0.01
D^S_{221221}	0	$-3.09 \cdot 10^4$	$5.50 \cdot 10^4$	$-3.86 \cdot 10^4$	$6.60 \cdot 10^3$	$7.99 \cdot 10^3$	3.87
D^S_{221122}	0	$-1.62 \cdot 10^4$	$2.48 \cdot 10^4$	$-1.36 \cdot 10^4$	$5.25 \cdot 10^3$	$-3.10 \cdot 10^2$	1.54
D^S_{221331}	0	$-1.34 \cdot 10^4$	$2.22 \cdot 10^4$	$-1.46 \cdot 10^4$	$3.77 \cdot 10^3$	$2.04 \cdot 10^3$	0.54
D^S_{221133}	$-2.41 \cdot 10^3$	$3.11 \cdot 10^3$	$-2.31 \cdot 10^3$	$1.92 \cdot 10^3$	$-3.64 \cdot 10^2$	$5.22 \cdot 10$	-0.04
D^S_{122122}	$2.82 \cdot 10^4$	$-8.27 \cdot 10^4$	$8.4 \cdot 10^4$	$-3.64 \cdot 10^4$	$7.37 \cdot 10^3$	$-4.41 \cdot 10^2$	1.14
D^S_{122133}	0	$9.66 \cdot 10^3$	$-1.50 \cdot 10^4$	$8.52 \cdot 10^3$	$-3.30 \cdot 10^3$	$1.13 \cdot 10^2$	-0.79
D^S_{231231}	0	$5.45 \cdot 10^3$	$-2.04 \cdot 10^4$	$1.65 \cdot 10^4$	$-5.27 \cdot 10^3$	$3.74 \cdot 10^3$	-3.96
D^S_{231132}	$8.33 \cdot 10^3$	$-2.63 \cdot 10^4$	$2.74 \cdot 10^4$	$-1.21 \cdot 10^4$	$2.98 \cdot 10^3$	$-2.26 \cdot 10^2$	0.50

example, rank 4 tensor parameters increase monotonously with the infill ratio. Hence, a topological weight reduction is possible as already implemented in commercial software solutions. But rank 6 tensor parameters behave differently. They present a peak around 60–80% infill ratio meaning that their dominance is maximized at this value. More importantly, the peak value of D^S_{111111} (around 65%) and D^S_{221221} (around 80%) are different. The former is a normal strain gradient along the same axis and the latter is the strain gradient along the orthogonal axis. In this way, dominance of the second gradient effect may be manipulated by choosing the infill ratio according to the loading scenario in an application. In general, the contribution of D^S is much weaker than C^S due to the fact that the microstructure fails to introduce a mechanism such as in a pantographic structure [45]. Therefore, second gradient is less pronounced; however, for a length scale near to the grid size, their contribution starts dominating. However, the optimization is more microstructural that is also possible

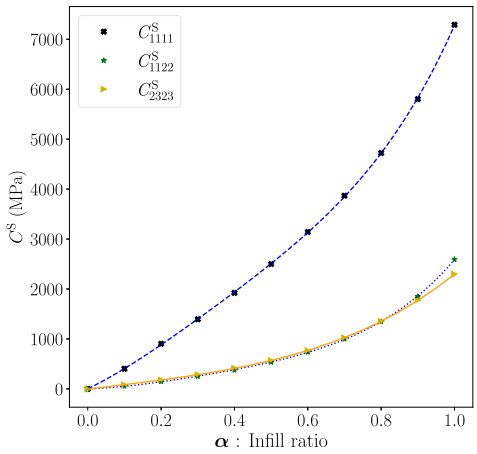

(a) Rank 4 tensor parameters and fit

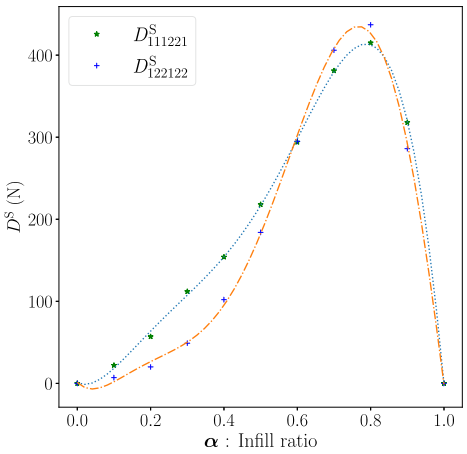

(b) Rank 6 tensor parameters and fit

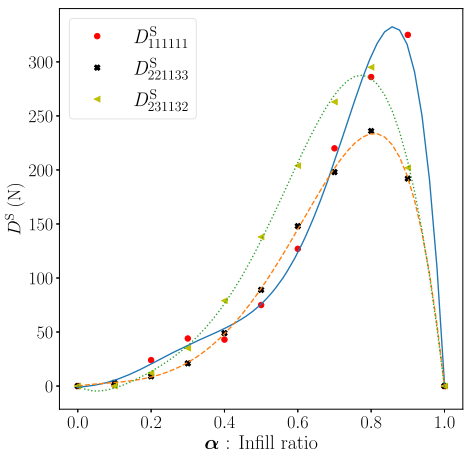

(c) Rank 6 tensor parameters and fit

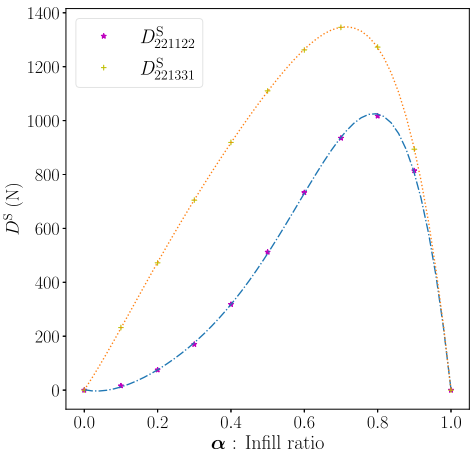

(d) Rank 6 tensor parameters and fit

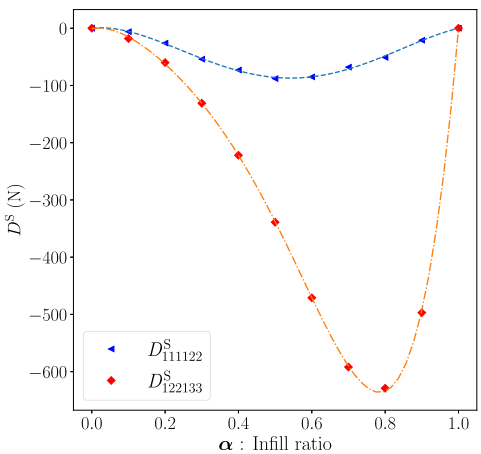

(e) Rank 6 tensor parameters and fit

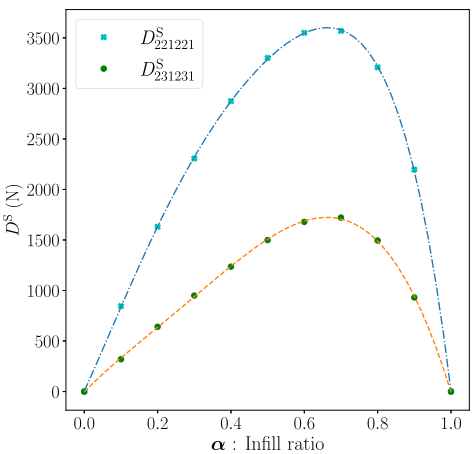

(f) Rank 6 tensor parameters and fit

Fig. 8 Determined constitutive parameters (dots) and infill ratio dependent functions (lines) fitting them, **a** for rank 4 and **b–f** for rank 6 parameters, due to the cubic symmetry only independent components are shown

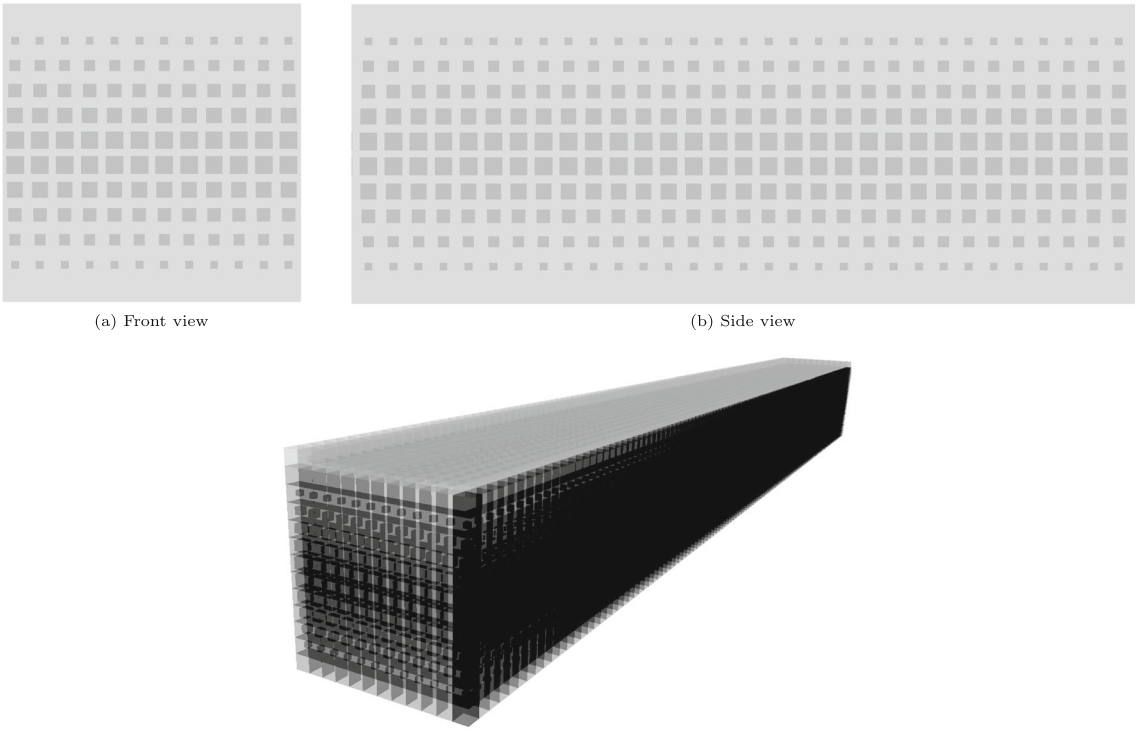

(a) Front view

(b) Side view

(c) Perspective view

Fig. 9 A conceptual presentation of a functionally gradient metamaterial design that is possible to analyze with the determined constitutive parameters of rank 4 and 6 tensors as a continuous function in infill ratio

with a topology optimization at the material scale, yet with a very high computational cost, in general not feasible for 3-D structures.

Furthermore, we proposed to fit the rank 4 and 6 tensors' parameters to the infill ratio, α, to reduce the complexity as well as allow for a study or an optimization of infill ratio within a structure. Therefore, we utilized the simplest polynomial function adequately describing all parameters. A 6-order polynomial fit has been successful, for a generic function for parameters, P, in the form:

$$P(\alpha) = A\alpha^6 + B\alpha^5 + C\alpha^4 + D\alpha^3 + E\alpha^2 + F\alpha + G\ . \tag{12}$$

Coefficient values are compiled in Table 1 and their fit to the simulation results are demonstrated in Fig. 8.

Since the fit functions represent the variation adequately, we conclude that a reduction of the microstructural effect to the scalar variable α is suitable. Such a variable is of utmost importance, not only because of being a manufacturing parameter but also due to its simplicity. One scalar variable represents the whole design space in additive manufacturing with infill ratio. In this way, an accurate prediction is possible with a computationally feasible simulation.

4 Conclusion

A strain gradient method is established as a multi-scale homogenization approach that is applied for an engineering composite material used in additive manufacturing. For a composite material, a homogenization needs to be used in order to decrease the computational cost. In 3-D printing, mostly for reducing weight, infill ratio is used as a standard manufacturing parameter in slicer that is preparing the G-code for the print. The methodology based on asymptotic homogenization is a useful strategy to increase the accuracy of predictions in a homogenized model without implementing ad-hoc assumptions.

For the investigated composite material with Carbon Black (CB) filled PolyLactic Acid (PLA), with realistic geometric dimensions, we found out that the composite material is homogenized adequately with a first-order theory (first-gradient material model) at the millimeter length-scale. However, at least for an increased accuracy,

infill ratio needs to be homogenized by incorporating a second-order theory (second-gradient material model). We have used the strain gradient elasticity and determined all parameters for several infill ratio. The complete design space is covered by reducing the complexity to the scalar variable called infill ratio, α, which is the manufacturing parameter such that we have demonstrated, probably for the first time in the literature, an accurate predictive material model with all parameters to be used in 3-D printing.

Consider a part in a product development phase. The part is designed with some restrictions such as connections to other parts. An engineer has a draft of the part that is functional and possible to manufacture, for example by 3-D printing. Yet a topology optimization may be needed to decrease the weight. Even if there are well-established methodologies, topology optimization is challenging to incorporate manufacturing restrictions. Instead, for the same CAD file and mesh, an infill ratio study may be done by using a strain gradient elasticity simulation [71–75].

Another possibility is to use such a varying infill ratio within the body. Functionally Graded Materials (FGM) [76,77] are widely used in product development [78], where their moduli varies in the product. Namely, rank 4 tensor parameters are a function in space. The same idea is possible to extend for a varying microstructure in order to develop a so-called programmable material for a specific loading scenario. We demonstrate an improvable discovery as a tailored material properties and focus on compositional graded structure whose grades are linearly changed in Fig. 9.

The application of porous structures has been adopted in biomedical engineering for implants and scaffolds. The porous structure has been prepared by Zhao et al [79] to increase the adsorption and metabolic movement of cells, promoting the growth of bone tissue cells. The designed femoral prosthesis by Perez-Boerema et al. [80] is characterized by periodic unsteady filling employing changing the gradient over the prosthesis additionally using unit cells having different characteristics. In mechanical engineering applications, functionally graded composites provide lightweight and gain crashworthiness during the designing of vehicles e.g in [81], Zhang et al. came up with a structural design having gradient porous to be used for bumper shock absorbers.

Declarations

Author contributions B.C.S., M.E.Y., and B.E.A. developed the concept. B.C.S. performed the numerical simulations and wrote the main manuscript. M.E.Y. and B.E.A. supervised the study. All the authors reviewed the manuscript.

Data availability No datasets were generated or analysed during the current study.

Conflict of interest The authors declare no conflict of interest.

References

1. Giorgio, I., Ciallella, A., Scerrato, D.: A study about the impact of the topological arrangement of fibers on fiber-reinforced composites: some guidelines aiming at the development of new ultra-stiff and ultra-soft metamaterials. Int. J. Solids Struct. **203**, 73–83 (2020)
2. Giorgio, I.: Lattice shells composed of two families of curved Kirchhoff rods: an archetypal example, topology optimization of a cycloidal metamaterial. Contin. Mech. Thermodyn. **33**(4), 1063–1082 (2021)
3. Turco, E., Giorgio, I., Misra, A., dell'Isola, F.: King post truss as a motif for internal structure of (meta) material with controlled elastic properties. R. Soc. Open Sci. **4**(10), 171153 (2017)
4. Aydin, G., Sarar, B.C., Yildizdag, M.E., Abali, B.E.: Investigating infill density and pattern effects in additive manufacturing by characterizing metamaterials along the strain-gradient theory. Math. Mech. Solids **27**(10), 2002–2016 (2022)
5. Wainwright, S.A., Biggs, W.D., Currey, J.D., Gosline, J.M.: Mechanical Design in Organisms. Princeton University Press, Princeton (1982)
6. Lekszycki, T., dell'Isola, F.: A mixture model with evolving mass densities for describing synthesis and resorption phenomena in bones reconstructed with bio-resorbable materials. ZAMM J. Appl. Math. Mech. Z. Angew. Math. Mech. **92**(6), 426–444 (2012)
7. Schaedler, T.A., Carter, W.B.: Architected cellular materials. Annu. Rev. Mater. Res. **46**, 187–210 (2016)
8. Yildizdag, M.E.: Numerical modeling and simulation of material extrusion-based 3-D printing processes with a material point method framework. Contin. Mech. Thermodyn. (2023). https://doi.org/10.1007/s00161-023-01273-1
9. Braides, A., Causin, A., Solci, M.: A homogenization result for interacting elastic and brittle media. Proc. R. Soc. A Math. Phys. Eng. Sci. **474**(2218), 20180118 (2018)
10. Rodrigues Lopes, I.A., Andrade Pires, F.M.: A fully second-order homogenization formulation for the multi-scale modeling of heterogeneous materials. Int. J. Numer. Meth. Eng. **123**(21), 5274–5318 (2022)

11. Barchiesi, E., dell'Isola, F., Seppecher, P., Turco, E.: A beam model for duoskelion structures derived by asymptotic homogenization and its application to axial loading problems. Eur. J. Mech. A Solids **98**, 104848 (2023)
12. Placidi, L., Barchiesi, E., Turco, E., Rizzi, N.L.: A review on 2D models for the description of pantographic fabrics. Z. Angew. Math. Phys. **67**, 1–20 (2016)
13. Kouznetsova, V., Geers, M.G., Brekelmans, W.: Multi-scale second-order computational homogenization of multi-phase materials: a nested finite element solution strategy. Comput. Methods Appl. Mech. Eng. **193**(48–51), 5525–5550 (2004)
14. Ameen, M.M., Peerlings, R., Geers, M.: A quantitative assessment of the scale separation limits of classical and higher-order asymptotic homogenization. Eur. J. Mech. A Solids **71**, 89–100 (2018)
15. Royer, P.: Low scale separation induces modification of apparent solute transport regime in porous media. Mech. Res. Commun. **87**, 29–34 (2018)
16. Mandadapu, K.K., Abali, B.E., Papadopoulos, P.: On the polar nature and invariance properties of a thermomechanical theory for continuum-on-continuum homogenization. Math. Mech. Solids **26**(11), 1581–1598 (2021)
17. Lesičar, T., Tonković, Z., Sorić, J.: Two-scale computational approach using strain gradient theory at microlevel. Int. J. Mech. Sci. **126**, 67–78 (2017)
18. Yalçınkaya, T., Çakmak, S.O., Tekoğlu, C.: A crystal plasticity based finite element framework for RVE calculations of two-phase materials: void nucleation in dual-phase steels. Finite Elem. Anal. Des. **187**, 103510 (2021)
19. Sarhil, M., Scheunemann, L., Schröder, J., Neff, P.: Size-effects of metamaterial beams subjected to pure bending: on boundary conditions and parameter identification in the relaxed micromorphic model. Comput. Mech. **72**, 1091–1113 (2023)
20. Yang, H., Timofeev, D., Giorgio, I., Müller, W.H.: Effective strain gradient continuum model of metamaterials and size effects analysis. Contin. Mech. Thermodyn. (2020). https://doi.org/10.1007/s00161-020-00910-3
21. Shekarchizadeh, N., Abali, B.E., Bersani, A.M.: A benchmark strain gradient elasticity solution in two-dimensions for verifying computational approaches by means of the finite element method. Math. Mech. Solids **27**(10), 2218–2238 (2022)
22. Molavitabrizi, D., Khakalo, S., Bengtsson, R., Mousavi, S.M.: Second-order homogenization of 3-D lattice materials towards strain gradient media: numerical modelling and experimental verification. Contin. Mech. Thermodyn. **35**(6), 2255–2274 (2023)
23. Yang, H., Liu, Z., Xia, Y., Fan, W., Taylor, A.C., Han, X.: Mechanical properties of hierarchical lattice via strain gradient homogenization approach. Compos. Part B Eng. **271**, 111153 (2023)
24. Mancusi, G., Fabbrocino, F., Feo, L., Fraternali, F.: Size effect and dynamic properties of 2D lattice materials. Compos. B Eng. **112**, 235–242 (2017)
25. Alibert, J.-J., Seppecher, P., dell'Isola, F.: Truss modular beams with deformation energy depending on higher displacement gradients. Math. Mech. Solids **8**(1), 51–73 (2003)
26. Seppecher, P., Alibert, J.-J., dell'Isola, F.: Linear elastic trusses leading to continua with exotic mechanical interactions. In: Journal of Physics: Conference Series, vol. 319, p. 012018. IOP Publishing (2011)
27. Turco, E., Dell'Isola, F., Rizzi, N.L., Grygoruk, R., Müller, W.H., Liebold, C.: Fiber rupture in sheared planar pantographic sheets: numerical and experimental evidence. Mech. Res. Commun. **76**, 86–90 (2016)
28. Turco, E., Golaszewski, M., Giorgio, I., D'Annibale, F.: Pantographic lattices with non-orthogonal fibres: experiments and their numerical simulations. Compos. B Eng. **118**, 1–14 (2017)
29. Placidi, L., Timofeev, D., Maksimov, V., Barchiesi, E., Ciallella, A., Misra, A., dell'Isola, F.: Micro-mechano-morphology-informed continuum damage modeling with intrinsic 2nd gradient (pantographic) grain-grain interactions. Int. J. Solids Struct. **254**, 111880 (2022)
30. Causin, A., Solci, M.: A singular limit of a family of variational evolutions for a brittle elastic bi-layer. Nonlinear Anal. **231**, 112949 (2023)
31. Alicandro, R., Braides, A., Cicalese, M., Solci, M.: Discrete Variational Problems with Interfaces. Cambridge Monographs on Applied and Computational Mathematics, Cambridge University Press, Cambridge (2023)
32. Cornacchia, F., Fabbrocino, F., Fantuzzi, N., Luciano, R., Penna, R.: Analytical solution of cross-and angle-ply nano plates with strain gradient theory for linear vibrations and buckling. Mech. Adv. Mater. Struct. **28**(12), 1201–1215 (2021)
33. Ciallella, A., D'Annibale, F., Del Vescovo, D., Giorgio, I.: Deformation patterns in a second-gradient lattice annular plate composed of "spira mirabilis" fibers. Contin. Mech. Thermodyn. **35**(4), 1561–1580 (2023)
34. Placidi, L., Andreaus, U., Corte, A.D., Lekszycki, T.: Gedanken experiments for the determination of two-dimensional linear second gradient elasticity coefficients. Z. Angew. Math. Phys. **66**(6), 3699–3725 (2015)
35. Lahbazi, A., Goda, I., Ganghoffer, J.-F.: Size-independent strain gradient effective models based on homogenization methods: applications to 3D composite materials, pantograph and thin walled lattices. Compos. Struct. **284**, 115065 (2022)
36. De Angelo, M., Yilmaz, N., Yildizdag, M.E., Misra, A., Hild, F., dell'Isola, F.: Identification and validation of constitutive parameters of a Hencky-type discrete model via experiments on millimetric pantographic unit cells. Int. J. Non Linear Mech. **153**, 104419 (2023)
37. Barchiesi, E., Misra, A., Placidi, L., Turco, E.: Granular micromechanics-based identification of isotropic strain gradient parameters for elastic geometrically nonlinear deformations. ZAMM J. Appl. Math. Mech. Z. Angew. Math. Mech. **101**(11), 202100059 (2021)
38. Lim, C., Zhang, G., Reddy, J.: A higher-order nonlocal elasticity and strain gradient theory and its applications in wave propagation. J. Mech. Phys. Solids **78**, 298–313 (2015)
39. Ayad, M., Karathanasopoulos, N., Ganghoffer, J.-F., Lakiss, H.: Higher-gradient and micro-inertia contributions on the mechanical response of composite beam structures. Int. J. Eng. Sci. **154**, 103318 (2020)
40. Ganghoffer, J., Reda, H.: A variational approach of homogenization of heterogeneous materials towards second gradient continua. Mech. Mater. **158**, 103743 (2021)
41. La Valle, G., Soize, C.: A higher-order nonlocal elasticity continuum model for deterministic and stochastic particle-based materials. Z. Angew. Math. Phys. **75**(2), 49 (2024)
42. Luciano, R., Darban, H., Bartolomeo, C., Fabbrocino, F., Scorza, D.: Free flexural vibrations of nanobeams with non-classical boundary conditions using stress-driven nonlocal model. Mech. Res. Commun. **107**, 103536 (2020)

43. Stilz, M., dell'Isola, F., Giorgio, I., Eremeyev, V.A., Ganzenmüller, G., Hiermaier, S.: Continuum models for pantographic blocks with second gradient energies which are incomplete. Mech. Res. Commun. **125**, 103988 (2022)
44. Stilz, M., Eugster, S.R., Harsch, J., Gutmann, F., Ganzenmüller, G., Hiermaier, S.: A second-gradient elasticity model and isogeometric analysis for the pantographic ortho-block. Int. J. Solids Struct. **280**, 112358 (2023)
45. Giorgio, I., dell'Isola, F., Steigmann, D.J.: Second-grade elasticity of three-dimensional pantographic lattices: theory and numerical experiments. Contin. Mech. Thermodyn. (2023). https://doi.org/10.1007/s00161-023-01240-w
46. Giorgio, I.: A discrete formulation of Kirchhoff rods in large-motion dynamics. Math. Mech. Solids **25**(5), 1081–1100 (2020)
47. Turco, E., dell'Isola, F., Cazzani, A., Rizzi, N.L.: Hencky-type discrete model for pantographic structures: numerical comparison with second gradient continuum models. Z. Angew. Math. Phys. **67**, 1–28 (2016)
48. Turco, E., Misra, A., Pawlikowski, M., dell'Isola, F., Hild, F.: Enhanced Piola–Hencky discrete models for pantographic sheets with pivots without deformation energy: numerics and experiments. Int. J. Solids Struct. **147**, 94–109 (2018)
49. Turco, E.: Discrete is it enough? The revival of Piola–Hencky keynotes to analyze three-dimensional Elastica. Contin. Mech. Thermodyn. **30**(5), 1039–1057 (2018)
50. Placidi, L., Barchiesi, E., dell'Isola, F., Maksimov, V., Misra, A., Rezaei, N., Scrofani, A., Timofeev, D.: On a hemi-variational formulation for a 2D elasto-plastic-damage strain gradient solid with granular microstructure. Math. Eng. **5**, 1–24 (2022)
51. Placidi, L., Barchiesi, E., Dell'Isola, F., Maksimov, V., Misra, A., Rezaei, N., Scrofani, A., Timofeev, D., et al.: A granular-based elasto-plastic–damage energy formulation for strain gradient solids. In: Book of Abstracts (2021)
52. Ciallella, A., Giorgio, I., Eugster, S.R., Rizzi, N.L., dell'Isola, F.: Generalized beam model for the analysis of wave propagation with a symmetric pattern of deformation in planar pantographic sheets. Wave Motion **113**, 102986 (2022)
53. Darban, H., Luciano, R., Caporale, A., Fabbrocino, F.: Higher modes of buckling in shear deformable nanobeams. Int. J. Eng. Sci. **154**, 103338 (2020)
54. Mühlich, U., Abali, B.E., dell'Isola, F.: Commented translation of Erwin Schrödinger's paper 'on the dynamics of elastically coupled point systems' (Zur Dynamik elastisch gekoppelter Punktsysteme). Math. Mech. Solids **26**(1), 133–147 (2021)
55. Abali, B.E., Barchiesi, E.: Additive manufacturing introduced substructure and computational determination of metamaterials parameters by means of the asymptotic homogenization. Contin. Mech. Thermodyn. **33**(4), 993–1009 (2021)
56. Vazic, B., Abali, B.E., Yang, H., Newell, P.: Mechanical analysis of heterogeneous materials with higher-order parameters. Eng. Comput. (2021). https://doi.org/10.1007/s00366-021-01555-9
57. Yang, H., Abali, B.E., Müller, W.H., Barboura, S., Li, J.: Verification of asymptotic homogenization method developed for periodic architected materials in strain gradient continuum. Int. J. Solids Struct. **238**, 111386 (2022)
58. Sarar, B.C., Yildizdag, M.E., Abali, B.E.: Comparison of homogenization techniques in strain gradient elasticity for determining material parameters. In: Sixty Shades of Generalized Continua: Dedicated to the 60th Birthday of Prof. Victor A. Eremeyev, pp. 631–644. Springer (2023)
59. Nazarenko, L., Glüge, R., Altenbach, H.: Uniqueness theorem in coupled strain gradient elasticity with mixed boundary conditions. Contin. Mech. Thermodyn. **34**(1), 93–106 (2022)
60. Nazarenko, L., Glüge, R., Altenbach, H.: Positive definiteness in coupled strain gradient elasticity. Contin. Mech. Thermodyn. **33**, 713–725 (2021)
61. Zohdi, T.I.: Finite Element Primer for Beginners. Springer, Berlin (2018)
62. Greco, L., Cuomo, M., Contrafatto, L.: Two new triangular G1-conforming finite elements with cubic edge rotation for the analysis of Kirchhoff plates. Comput. Methods Appl. Mech. Eng. **356**, 354–386 (2019)
63. Abali, B.E.: Computational Reality. Advanced Structured Materials, vol. 55. Springer, Berlin (2017)
64. Auffray, N., He, Q.-C., Le Quang, H.: Complete symmetry classification and compact matrix representations for 3D strain gradient elasticity. Int. J. Solids Struct. **159**, 197–210 (2019)
65. Auffray, N., Le Quang, H., He, Q.-C.: Matrix representations for 3D strain-gradient elasticity. J. Mech. Phys. Solids **61**(5), 1202–1223 (2013)
66. Abali, B.E., Vazic, B., Newell, P.: Influence of microstructure on size effect for metamaterials applied in composite structures. Mech. Res. Commun. (2022). https://doi.org/10.1016/j.mechrescom.2022.103877
67. dell'Isola, F., Seppecher, P., Alibert, J.J., Lekszycki, T., Grygoruk, R., Pawlikowski, M., Steigmann, D., Giorgio, I., Andreaus, U., Turco, E., Golaszewski, M., Rizzi, N., Boutin, C., Eremeyev, V.A., Misra, A., Placidi, L., Barchiesi, E., Greco, L., Cuomo, M., Cazzani, A., Della Corte, A., Battista, A., Scerrato, D., Eremeeva, I.Z., Rahali, Y., Ganghoffer, J.-F., Muller, W., Ganzosch, G., Spagnuolo, M., Pfaff, A., Barcz, K., Hoschke, K., Neggers, J., Hild, F.: Pantographic metamaterials: an example of mathematically driven design and of its technological challenges. Contin. Mech. Thermodyn. **31**, 851–884 (2019)
68. dell'Isola, F., Seppecher, P., Spagnuolo, M., Barchiesi, E., Hild, F., Lekszycki, T., Giorgio, I., Placidi, L., Andreaus, U., Cuomo, M., Eugster, S.R., Pfaff, A., Hoschke, K., Langkemper, R., Turco, E., Sarikaya, R., Misra, A., De Angelo, M., D'Annibale, F., Bouterf, A., Pinelli, X., Misra, A., Desmorat, B., Pawlikowski, M., Dupuy, C., Scerrato, D., Peyre, P., Laudato, M., Manzari, L., Göransson, P., Hesch, C., Hesch, S., Franciosi, P., Dirrenberger, J., Maurin, F., Vangelatos, Z., Grigoropoulos, C., Melissinaki, V., Farsari, M., Muller, W., Abali, B.E., Liebold, C., Ganzosch, G., Harrison, P., Drobnicki, R., Igumnov, L., Alzahrani, F., Hayat, T.: Advances in pantographic structures: design, manufacturing, models, experiments and image analyses. Contin. Mech. Thermodyn. **31**(4), 1231–1282 (2019)
69. Spagnuolo, M., Andreaus, U., Misra, A., Giorgio, I., Hild, F.: Mesoscale modeling and experimental analyses for pantographic cells: effect of hinge deformation. Mech. Mater. **160**, 103924 (2021)
70. dell'Isola, F., Misra, A.: Principle of virtual work as foundational framework for metamaterial discovery and rational design. C. R. Méc. **351**(S3), 1–25 (2023)
71. Abali, B.E., Müller, W.H., dell'Isola, F.: Theory and computation of higher gradient elasticity theories based on action principles. Arch. Appl. Mech. **87**(9), 1495–1510 (2017). https://doi.org/10.1007/s00419-017-1266-5
72. Khakalo, S., Niiranen, J.: Isogeometric analysis of higher-order gradient elasticity by user elements of a commercial finite element software. Comput. Aided Des. **82**, 154–169 (2017)
73. Makvandi, R., Reiher, J.C., Bertram, A., Juhre, D.: Isogeometric analysis of first and second strain gradient elasticity. Comput. Mech. **61**, 351–363 (2018)

74. Greco, L., Cuomo, M., Contrafatto, L.: A quadrilateral G1-conforming finite element for the Kirchhoff plate model. Comput. Methods Appl. Mech. Eng. **346**, 913–951 (2019)
75. Hosseini, S., Niiranen, J.: 3D strain gradient elasticity: variational formulations, isogeometric analysis and model peculiarities. Comput. Methods Appl. Mech. Eng. **389**, 114324 (2022)
76. Abali, B.E., Völlmecke, C., Woodward, B., Kashtalyan, M., Guz, I., Müller, W.H.: Numerical modeling of functionally graded materials using a variational formulation. Contin. Mech. Thermodyn. **24**(4), 377–390 (2012)
77. Abali, B.E., Völlmecke, C., Woodward, B., Kashtalyan, M., Guz, I., Müller, W.H.: Three-dimensional elastic deformation of functionally graded isotropic plates under point loading. Compos. Struct. **118**, 367–376 (2014). https://doi.org/10.1016/j.compstruct.2014.07.013
78. Njim, E.K., Al-Waily, M., Bakhy, S.H.: A review of the recent research on the experimental tests of functionally graded sandwich panels. J. Mech. Eng. Res. Dev. **44**(3), 420–441 (2021)
79. Zhao, L., Pei, X., Jiang, L., Hu, C., Sun, J., Xing, F., Zhou, C., Fan, Y., Zhang, X.: Bionic design and 3D printing of porous titanium alloy scaffolds for bone tissue repair. Compos. B Eng. **162**, 154–161 (2019)
80. Zhu, Y., Zhu, R., Ma, J., Weng, Z., Wang, Y., Shi, X., Li, Y., Yan, X., Dong, Z., Xu, J., et al.: In vitro cell proliferation evaluation of porous nano-zirconia scaffolds with different porosity for bone tissue engineering. Biomed. Mater. **10**(5), 055009 (2015)
81. Zhang, Y., Xu, X., Liu, S., Chen, T., Hu, Z.: Crashworthiness design for bi-graded composite circular structures. Constr. Build. Mater. **168**, 633–649 (2018)